Mapping subsurface scatterers from SAR backscatter time series

Wolfgang Wagner[a,b], Bernhard Raml[a], Roland Lindorfer[a], Martin Schobben[a], Samuel Massart[a], Mariette Vreugdenhil[a], Tobias Stachl[b], Senmao Cao[b], and Tobias Ullmann[c]
[a]Technische Universität Wien, Department of Geodesy and Geoinformation, Vienna, Austria
[b]EODC Earth Observation Data Centre, Vienna, Austria
[c]Julius-Maximilians-Universität Würzburg, Department of Remote Sensing, Würzburg, Germany

Abstract

Microwave pulses transmitted by Synthetic Aperture Radars (SAR) penetrate several centimetres to decimetres into dry soil. Even at the comparably short wavelength of the SAR instrument mounted onboard the Sentinel-1 satellites (C-band, 5.6 cm), dielectric discontinuities in the soil profile can give rise to strong subsurface scattering signals that dominate the returns from the soil surface. In such situations, backscatter decreases when the soils get wet because the damping of subsurface scattering signals is more important than the increased backscatter from the soil surface. By comparing backscatter time series with modelled soil moisture data, this characteristic behaviour can be detected, opening up the possibility of using SAR data for mapping subsurface scatterers at high spatial resolution. This contribution introduces an index for mapping surface scatterers using a global Sentinel-1 backscatter datacube. We computed the index over a study region covering the Iberian Peninsula and north-western Africa, which was the focus of a previous study using the Advanced Scatterometer (ASCAT). The results show that the Sentinel-1-based index reflects large-scale patterns of subsurface scattering as detected by ASCAT very well. At local scales, the Sentinel-1 maps reveal patterns related to soil and landscape features in much more detail than depicted by currently available soil maps.

1 Introduction

Soils are vital for life on Earth, playing a crucial role in meeting fundamental human necessities such as nourishing food, providing clean water, and fostering biodiversity [1]. Unfortunately, mapping the quality of soils with in situ techniques is arduous due to the large heterogeneity of soils, and suitable monitoring methodologies being expensive or non-existent [2]. Consequently, there has been much interest in using remote sensing data for soil mapping. So far, most efforts have focused on using multispectral and hyperspectral imagery providing spectral information on the chemical composition of the soil, which in turn can be used as indirect proxy in predictive soil mapping [3, 4]. Combined with Artificial Intelligence (AI) techniques, these optical data have enabled a revolution in soil mapping, yielding high-resolution soil maps at continental to global scales [5, 6]. Still, the disadvantage of sensors using the visible and infrared portion of the electromagnetic spectrum is that they cannot sense subsurface soil properties, and are blocked by vegetation. This means that optical data can not provide direct information about soil profile properties.

These shortcomings can be overcome by using Synthetic Aperture Radar (SAR) sensors that penetrate soil and vegetation to some extent. The penetration depth into the soil is in the order of a wavelength, i.e., a few centimetres to decimetres at commonly used SAR frequencies (e.g. X, C, L-band). However, the penetration varies strongly with the water content in the soil profile, whereas it is only a fraction of the wavelength for wet soils, and multiple wavelengths for dry soils. Particularly in arid regions, penetration depths may be quite large, allowing to map bedrock and gravel surfaces beneath several centimetres to possibly meters thick windblown sand [7, 8]. Experimental measurements of radar transmission through sand from P- to X-band (0.5–12.6 GHz) revealed that dry sand resulted in attenuations of less than 6 dB/m over the entire frequency range [9]. Even under moister conditions (4.7 and 10.7 vol%), the penetration was quite large for the lower frequencies (L- and P-band). Therefore, Williams and Greeley [9] challenged the notion that sand must be extremely dry for radar penetration to occur.

As a result, SAR measurements are sensitive to dielectric discontinuities in the soil profile caused by the presence of stones, rocks or distinct soil horizons. These discontinuities may constitute quite effective subsurface scatterers that cause strong backscatter when the soil is dry. However, when the soil gets wet, the attenuation of the microwave pulses through the intermediate soil layers increases, which causes backscatter as measured by radar to decrease [10, 11]. This characteristic behaviour can be detected by comparing backscatter time series with in situ or modelled soil moisture time series, allowing to map subsurface scatterers using spaceborne radar sensors [12].

The conditions for detecting subsurface scattering signals are ideal in arid environments, where soils are dry and usually poorly developed. Nevertheless, a global-scale analysis of multi-year C-band backscatter time series acquired by the Advanced Scatterometer (ASCAT) has shown that subsurface scatterers can also be detected in more humid environments during dry periods [13]. Therefore, this

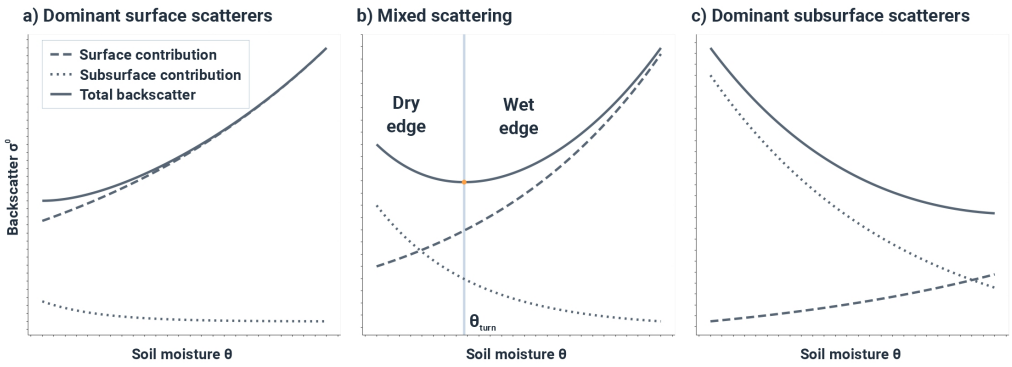

Figure 1 Backscattering behaviour of bare soil with (a) dominant surface, (b) mixed, and (c) dominant subsurface scatterers. Figure 3 from [12] (CC BY license).

study aims to explore the capability of Sentinel-1 to map soil profile properties at high resolution over a wide range of environmental conditions. The analysis was carried out over a study region covering the Iberian Peninsula and north-western Africa which was the focus of a previous study with ASCAT [12]. This area covers a wide range of environmental conditions governing subsurface scattering, from hyperarid regions in the Sahara with strong and permanent subsurface signals, to semi-arid conditions in central and south-eastern Spain with weaker, intermittent anomalies.

2 Method

As described above, subsurface scatterers can be detected by their characteristic backscatter response to changing soil moisture conditions. When the soil is evenly textured without major inclusions of stones or distinct soil layers, then the volume scattering contribution from the soil profile is small [14], and backscatter increases monotonically with the soil moisture content (Figure 1a). However, if there are strong subsurface scatterers (e.g. crusts), then backscatter decreases with increasing soil moisture as the damping of the contributions from deeper soil layers is more important than the increasing scattering contribution from the soil surface. This can lead to an initial decrease of backscatter for dry soil conditions (Figure 1b), or to a complete reversal of the backscatter-soil moisture relationship for brightly reflecting subsurface discontinuities (Figure 1c).

This reversed relationship – an "anomaly" from the point of view of soil moisture and vegetation retrievals – can be detected by comparing backscatter time series to external soil moisture data such as that derived from ERA5-Land [15]. When collocating ASCAT backscatter and ERA5-Land soil moisture time series, it is possible to use a physically based approach in which two semi-empirical models – one with and one without a subsurface scattering term – are fitted to the collocated data, and the best-fitting model is selected [12]. The advantage of this approach is, that it is a physically based approach that provides an estimate of the strength of the subsurface scattering signals. However, it is a rather complex method that is not very robust to data outliers and differences in signal dynamics apparent in the ASCAT and ERA5-Land data [13].

On the other hand, robust results have been obtained with a simple statistical method that searches the time series for strong negative correlations between the backscatter and soil moisture values. It is calculated by computing the Spearman's rank correlation for a sliding time window of one month (31 days), and by determining how frequently ρ falls below a certain threshold. This yields an estimate of the probability of the occurrence of backscatter anomalies

$$\mathcal{P}_{ano} = \frac{N\left(\rho < -0.4\right)}{N_{total}} \tag{1}$$

where N is the number of days when ρ is smaller than the threshold (-0.4), and N_{total} is the total number of days within the considered time frame. In principle, the time frame can be chosen arbitrarily but should not be too short to yield statistically meaningful results. In this study, we computed $\mathcal{P}_{ano}$ for ASCAT data acquired over 15 years from 2007–2021.

As can be seen from the global $\mathcal{P}_{ano}$ map shown in Figure 2, subsurface scattering is not only widespread in arid regions (deserts), but also in more humid climates with a dry season. Along with the soil's dryness, coarse fragments in the soil profile, and sparse vegetation cover are important factors favouring its occurrence [13]. Unfortunately, a direct transfer of this second method from ASCAT to Sentinel-1 is impossible due to the much lower temporal sampling rate of Sentinel-1, and its Petabyte-scale data volume. As described in [16], the challenges posed by the large data volume can be solved using a streaming approach. This involves interleaving data reading and processing, using Pearson's correlation r instead of Spearman's rank correlation, as the former can be calculated iteratively. To deal with large biases between the Sentinel-1 orbits, r is first calculated separately for each orbit, and then averaged over all orbits weighted by the number of observations. The so-derived average $\overline{r}$ value is then used to compute R_{sub}, defined as:

$$R_{sub} = \begin{cases} |\overline{r}| & \text{if } r < 0 \\ 0 & \text{if } r \geq 0 \end{cases} \tag{2}$$

where $|\overline{r}|$ is the absolute value of $\overline{r}$. Thereby, R_{sub} takes on values between 0 (0%) and 1 (100%) which can be intu-

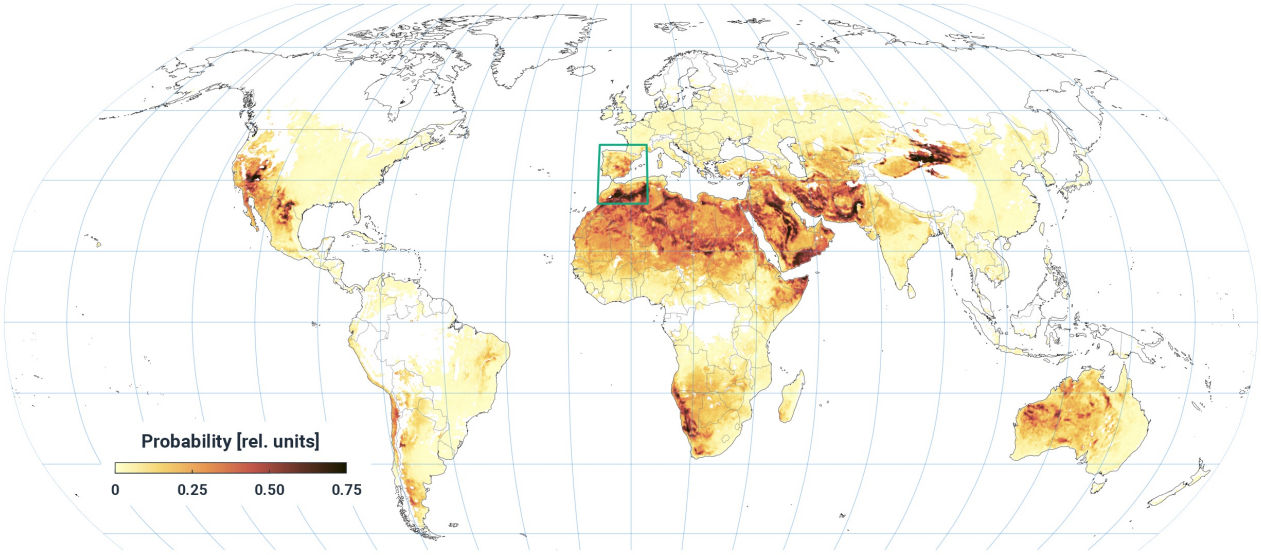

Figure 2 The probability of the occurrence of subsurface scattering derived from analysing ASCAT backscatter time series from the years 2007 to 2021 [13]. The green rectangle shows the location of the study area.

itively interpreted as an indicator of subsurface scattering strength. Specifically, values equal to or near zero indicate no subsurface scattering, while high values suggest dominant subsurface scattering.

3 Results

Sentinel-1-based subsurface scattering maps were produced over the study area (10°W to 5°E, 30°N to 45°N) by analysing backscatter data acquired by Sentinel-1A and Sentinel-1B in the years from 2017 to 2021. ERA5-Land soil moisture data ("Volumetric soil water layer 1") were collocated to the backscatter time series by resampling the ERA5-Land data to the 20m Equi7Grid [17] used for the Sentinel-1 backscatter datacube [18], and selecting the ERA5-Land data timestamp closest to the Sentinel-1 acquisition [16]. The derived R_{sub} maps exhibit rich spatial details following important landscape features such as mountain ranges or different types of desert landforms (Figure 3f).

Unfortunately, a quantitative validation of R_{sub} is difficult due to the lack of suitable ground observations. Therefore, in this exploratory study, we confine ourselves to comparing the R_{sub} maps to $\mathcal{P}_{ano}$, and selected environmental variables that have been found to be useful for explaining the occurrence of subsurface scattering (Figure 3). This selection consists of the mean soil moisture content computed from ERA5-Land, the mean leaf area index (LAI) from Copernicus [19], and the fraction of coarse fragments (CFVO) in the 5-15 cm soil layer from SoilGrids250m [20]. Furthermore, given that several of the subsurface scattering areas follow the topography of mountain ranges situated in the arid parts of the study region quite well (e.g., Atlas Mountains in Morocco, Baetic Mountain Ranges in the arid south-east of Spain), elevation was extracted from the Copernicus Digital Elevation Model [21].

The R_{sub} averaged to the ASCAT scale shows a good correspondence to the $\mathcal{P}_{ano}$ values from ASCAT (Figure 3e). Pearson's correlation r between the two indicators is 0.8 ($p < 0.001$), suggesting a significant and positive linear association between the subsurface scattering indicators. Both R_{sub} and P_{ano} also exhibit the expected dependencies on the selected environmental variables, whereas the association to mean soil moisture and mean LAI is strongest (Table 1). Over the study area, elevation also explains some of the spatial variability of the two subsurface scattering indicators, while there is no clear relationship to CFVO (contrary to what was found at global scale [13]). In all instances, the correlation is smaller for R_{sub} than for P_{ano}. Nonetheless, given that the number of ASCAT measurements is significantly higher than for Sentinel-1, and given the differences in the methodologies, this is deemed a good result demonstrating that Sentinel-1 can be used to detect backscatter anomalies caused by subsurface scatterers.

Table 1 Pearson correlation r (Clifford-Richardson's solution) and p-value (in brackets)

	$\mathcal{P}_{ano}$	R_{sub}
Elevation	0.4 (0.003)	0.24 (0.04)
Leaf area index	-0.75 (0.021)	-0.51 (0.059)
Soil moisture	-0.83 (<0.001)	-0.58 (0.036)
Coarse fragments	0.19 (0.187)	0.13 (0.277)
Observations	8,843	8,843

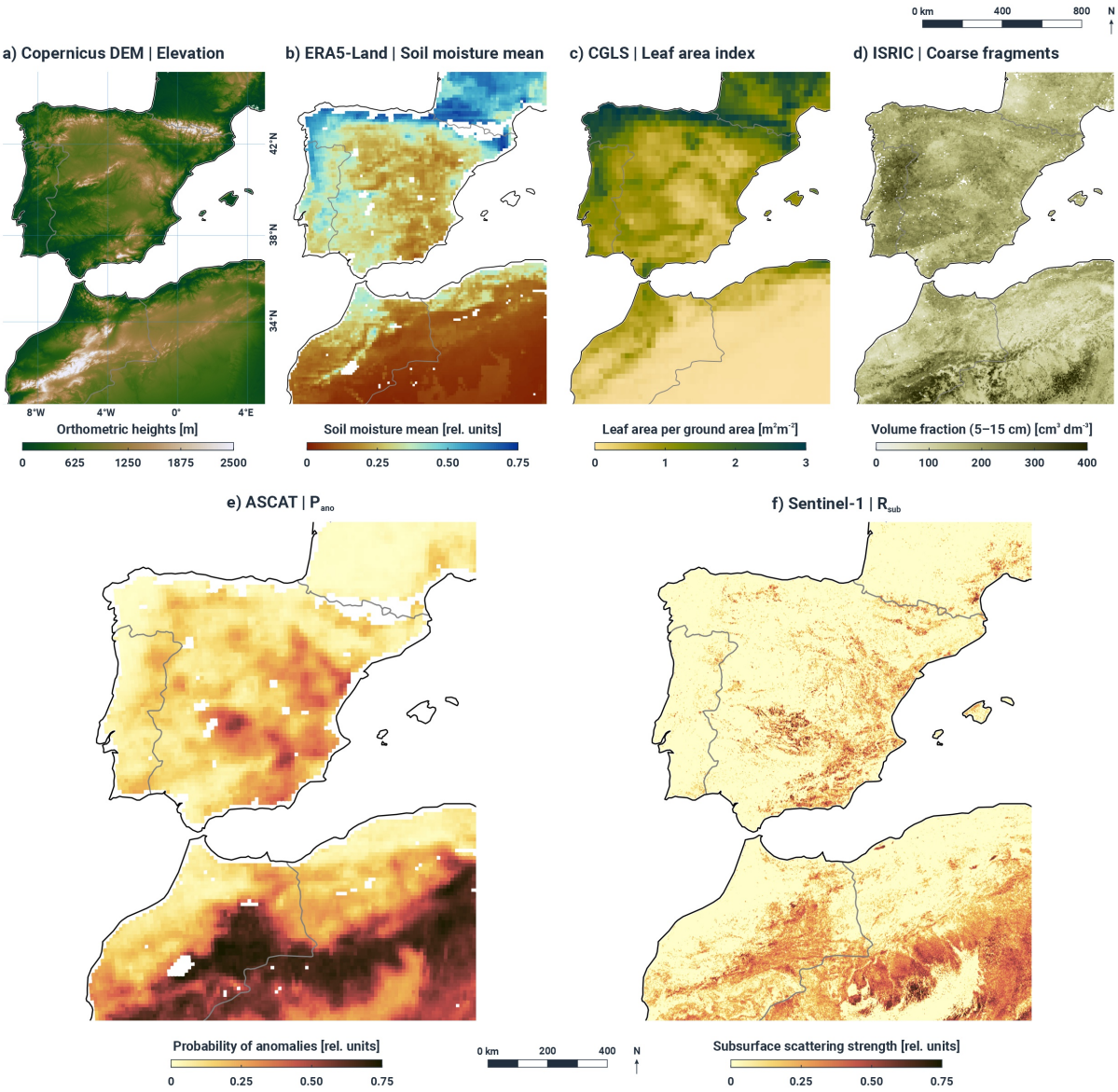

Figure 3 A comparison of the subsurface scattering maps derived from ASCAT (lower left) and Sentinel-1 (lower right) with different environmental variables: (a) elevation from Copernicus DEM, (b) mean soil moisture from ERA5-Land, (c) mean leaf area index from Copernicus Global Land Service (CGLS), (d) coarse fragments in 5-15 cm soil layer from ISRIC SoilGrids250m.

4 Conclusions

In this paper, we introduced a SAR-based indicator of subsurface scattering strengths, R_{sub}, that takes on values between 0 (no subsurface scattering) and 1 (strong subsurface scattering). The comparison to ASCAT and selected environmental variables showed that the Sentinel-1-based index reflects the large-scale patterns of subsurface scattering, as detected by ASCAT, well. At local scales, the Sentinel-1 maps reveal patterns related to soil and landscape features that are much more detailed than depicted by currently available soil maps. As some of the local-scale features may come from non-soil-related backscatter anomalies (e.g. crop phenology, surface water, wet snow), future work will have to investigate means to mask these non-subsurface-scattering related signals. Moreover, research is needed to establish connections between R_{sub} and physical soil characteristics, whereat generic associations to soil groups, soil depth, or the fraction of coarse fragments within the soil profile would be most useful. This will be challenging due to the scarcity of suitable ground observations and the highly correlated nature of the environmental processes that lead to subsurface scattering phenomena.

5 Acknowledgements

Co-funding from the DTE Hydrology project funded by the European Space Agency (Contract 4000129870/20/I-NB) and the ROSSIHNI project funded by the Austrian Space Applications Programme (FFG Pr.No. FO999892643) is gratefully acknowledged.

6 Literature

[1] L. Montanarella et al., "World's soils are under threat," SOIL, vol. 2, no. 1, pp. 79–82, Feb. 2016, doi: 10.5194/soil-2-79-2016.

[2] S. D. Keesstra et al., "The significance of soils and soil science towards realization of the United Nations Sustainable Development Goals," SOIL, vol. 2, no. 2, pp. 111–128, Apr. 2016, doi: 10.5194/soil-2-111-2016.

[3] V. L. Mulder, S. De Bruin, M. E. Schaepman, and T. R. Mayr, "The use of remote sensing in soil and terrain mapping — A review," Geoderma, vol. 162, no. 1–2, pp. 1–19, Apr. 2011, doi: 10.1016/j.geoderma.2010.12.018.

[4] P. Scull, J. Franklin, O. A. Chadwick, and D. McArthur, "Predictive soil mapping: a review," Progress in Physical Geography: Earth and Environment, vol. 27, no. 2, pp. 171–197, Jun. 2003, doi: 10.1191/0309133303pp366ra.

[5] T. Hengl et al., "Mapping Soil Properties of Africa at 250 m Resolution: Random Forests Significantly Improve Current Predictions," PLoS ONE, vol. 10, no. 6, p. e0125814, Jun. 2015, doi: 10.1371/journal.pone.0125814.

[6] N. Tziolas et al., "Earth Observation Data-Driven Cropland Soil Monitoring: A Review," Remote Sensing, vol. 13, no. 21, p. 4439, Nov. 2021, doi: 10.3390/rs13214439.

[7] J. F. McCauley et al., "Subsurface Valleys and Geoarcheology of the Eastern Sahara Revealed by Shuttle Radar," Science, vol. 218, no. 4576, pp. 1004–1020, Dec. 1982, doi: 10.1126/science.218.4576.1004.

[8] G. Schaber, J. McCauley, C. Breed, and G. Olhoeft, "Shuttle Imaging Radar: Physical Controls on Signal Penetration and Subsurface Scattenng in the Eastern Sahara," IEEE Trans. Geosci. Remote Sensing, vol. GE-24, no. 4, pp. 603–623, Jul. 1986, doi: 10.1109/TGRS.1986.289677.

[9] K. K. Williams and R. Greeley, "Radar attenuation by sand: laboratory measurements of radar transmission," IEEE Trans. Geosci. Remote Sensing, vol. 39, no. 11, pp. 2521–2526, Nov. 2001, doi: 10.1109/36.964990.

[10] P.-W. Liu, J. Judge, R. D. DeRoo, A. W. England, T. Bongiovanni, and A. Luke, "Dominant backscattering mechanisms at L-band during dynamic soil moisture conditions for sandy soils," Remote Sensing of Environment, vol. 178, pp. 104–112, Jun. 2016, doi: 10.1016/j.rse.2016.02.062.

[11] K. Morrison and W. Wagner, "Explaining Anomalies in SAR and Scatterometer Soil Moisture Retrievals From Dry Soils With Subsurface Scattering," IEEE Trans. Geosci. Remote Sensing, vol. 58, no. 3, pp. 2190–2197, Mar. 2020, doi: 10.1109/TGRS.2019.2954771.

[12] W. Wagner et al., "Widespread occurrence of anomalous C-band backscatter signals in arid environments caused by subsurface scattering," Remote Sensing of Environment, vol. 276, p. 113025, Jul. 2022, doi: 10.1016/j.rse.2022.113025.

[13] W. Wagner et al., "Global scale mapping of subsurface scattering signals impacting ASCAT soil moisture retrievals," TechRxiv. Preprint.

[14] E. Schanda, "On the contribution of volume scattering to the microwave backscattered signal from wet snow and wet soil," International Journal of Remote Sensing, vol. 8, no. 10, pp. 1489–1500, Oct. 1987, doi: 10.1080/01431168708954791.

[15] J. Muñoz-Sabater et al., "ERA5-Land: a state-of-the-art global reanalysis dataset for land applications," Earth Syst. Sci. Data, vol. 13, no. 9, pp. 4349–4383, Sep. 2021, doi: 10.5194/essd-13-4349-2021.

[16] B. Raml, M. Vreugdenhil, S. Massart, C. Navacchi, and W. Wagner, "Enabling global scale Sentinel-1 time series analysis through streaming," BiDS Proceedings, 2023, submitted.

[17] B. Bauer-Marschallinger, D. Sabel, and W. Wagner, "Optimisation of global grids for high-resolution remote sensing data," Computers & Geosciences, vol. 72, pp. 84–93, Nov. 2014, doi: 10.1016/j.cageo.2014.07.005.

[18] W. Wagner et al., "A Sentinel-1 Backscatter Datacube for Global Land Monitoring Applications," Remote Sensing, vol. 13, no. 22, p. 4622, Nov. 2021, doi: 10.3390/rs13224622.

[19] Copernicus Climate Change Service, "Leaf area index and fraction absorbed of photosynthetically active radiation 10-daily gridded data from 1981 to present." ECMWF, 2018. doi: 10.24381/CDS.7E59B01A.

[20] T. Hengl et al., "SoilGrids250m: Global gridded soil information based on machine learning," PLoS ONE, vol. 12, no. 2, p. e0169748, Feb. 2017, doi: 10.1371/journal.pone.0169748.

[21] European Space Agency and Airbus, "Copernicus DEM." 2022. doi: 10.5270/ESA-c5d3d65.